PHYSICAL REVIEW B **93**, 241303(R) (2016)

Electronic structure near the Fermi level in the ferromagnetic semiconductor GaMnAs studied by ultrafast time-resolved light-induced reflectivity measurements

Tomoaki Ishii,[1] Tadashi Kawazoe,[1] Yusuke Hashimoto,[2] Hiroshi Terada,[1] Iriya Muneta,[1] Motoichi Ohtsu,[1] Masaaki Tanaka,[1,3] and Shinobu Ohya[1,3]

[1]*Department of Electrical Engineering and Information Systems, The University of Tokyo, 7-3-1 Hongo, Bunkyo-ku, Tokyo 113-8656, Japan*

[2]*WPI Advanced Institute for Materials Research, Tohoku University, 2-1-1 Katahira, Aoba-ku, Sendai 980-8577, Japan*

[3]*Center for Spintronics Research Network, Graduate School of Engineering, The University of Tokyo, 7-3-1 Hongo, Bunkyo-ku, Tokyo 113-8656, Japan*

(Received 15 December 2015; revised manuscript received 3 May 2016; published 14 June 2016)

Clarification of the electronic structure near the Fermi level is important in understanding the origin of ferromagnetism in the prototypical ferromagnetic semiconductor GaMnAs. Here, we perform ultrafast transient reflectivity spectra measurement, which is a powerful tool for selective detection of absorption edges in GaMnAs. The results show that the Fermi level of GaMnAs exists in the band gap. By using the Kramers-Kronig relation, we find the Mn-induced electronic states around the Fermi level, confirming that the ferromagnetism is stabilized by spin-polarized impurity-band holes.

DOI: 10.1103/PhysRevB.93.241303

GaMnAs is a prototypical ferromagnetic semiconductor that exhibits intriguing features originating from the interplay between ferromagnetic and semiconducting properties [1,2]. Although GaMnAs is the most investigated ferromagnetic semiconductor, its band structure and the origin of its ferromagnetism are still under debate. Over the past few years, the nature of the ferromagnetism of GaMnAs has been widely studied, with significant focus on the position of the Fermi level [3–16]. Recent experimental studies, including resonant tunneling [3,4], magnetic circular dichroism [5,6], and angle-resolved photoemission [7] experiments, concluded that the Fermi level of GaMnAs exists in the Mn-induced impurity band (IB) inside the band gap [8–12]. In this case, the ferromagnetism of GaMnAs is thought to be stabilized by spin-polarized IB holes [3,4,10]. There are also reports claiming that the Fermi level exists in the valence band (VB) [1,13–16]. In this case, the ferromagnetism would be induced by the itinerant spin-polarized VB holes; this spin polarization is due to *p*-*d* exchange interactions with localized *d* electrons [1]. Linear optical spectroscopy (LOS), which observes the absorption or transmission spectrum, has been widely used to investigate the band structure of semiconductors. However, in the case of GaMnAs, the LOS spectrum shows a broad peak at a photon energy close to the band gap, due to the overlap of the IB and the VB. Thus, it is difficult to determine the position of the Fermi level using LOS [11,17].

Here, we investigate the electronic structure near the Fermi level in GaMnAs through measurement of the transient reflectivity spectrum (TRS). We suggest that the TRS provides the effective means to determine the energy of the absorption edges as explained below [18]. The band structure of GaAs is schematically shown in Fig. 1(a). There is an absorption edge E_g corresponding to the optical transition from the top of the VB to the bottom of the conduction band (CB) [Fig. 1(a)]. In GaMnAs, due to the Mn-induced IB, there is another absorption edge E_F corresponding to the optical transition from the Fermi level to the bottom of the CB [Fig. 1(b)]. We note that this band picture is supported by recent studies of resonant tunneling spectroscopy and the angle-resolved photoemission spectroscopy, in which researchers observed a sharp VB overlapped with the disordered and energetically broad IB [3,4,7,19–23]. In TRS experiments on GaMnAs, photocarriers are generated in the CB, VB, and IB by the illumination of a pump pulse, and the excited carriers relax to the band edges and to the Fermi level in the time scale of tens of picoseconds [24]. Thus, the transient reflectivity signal after 100 ps directly represents the photocarriers that are placed at the band edges and the Fermi level. The TRS measurement is thus sensitive to the absorption edges. Here, we analyze the signals using a model considering a combination of band-gap renormalization (BGR) and band filling (BF) [25,26]. Although a similar study was reported in Ref. [16], the excitation fluence, and thus the accumulation of photocarriers, was rather high; this can change the band structure because the BGR and/or BF [27] are too strong.

In this Rapid Communication, we demonstrate TRS measurements on a series of $Ga_{1-x}Mn_xAs$ samples, in which the Mn concentration x is systematically varied from 0.1% to 6%. The pump pulse fluence was carefully chosen to avoid the aforementioned high-excitation effect. Our measurements show that the Fermi level is located in the band gap for all $Ga_{1-x}Mn_xAs$ films examined in our study, and that there are Mn-induced electronic states around the Fermi level. Thus, our results support the IB conduction picture.

Time-resolved reflectivity measurements were performed using a degenerate (single-color) pump-probe technique. An 80-MHz picosecond pulsed laser, with a time duration of 3 ps, was chosen as the light source. Using the picosecond laser, a high energy resolution of 0.5 meV, which is much higher than in the previous studies using femtosecond pulses (∼10 meV) [9,16], was achieved with a photodiode and a simple lock-in technique [see Sec. A of the Supplemental Material (SM) [28]]. The TRS was measured by changing the wavelength of the source laser. In our measurements, the fluences of the pump and probe pulses were 160 and 1 nJ/cm^2, respectively. The density of photocarriers in the GaMnAs film was estimated to be 8×10^{15} cm^{-3} by assuming that light penetrates into the sample at a distance of 800 nm from the surface. This photocarrier density is three orders of magnitude smaller than that in the previous study (∼10^{19} cm^{-3}) [16], thus

 ©2016 American Physical Society

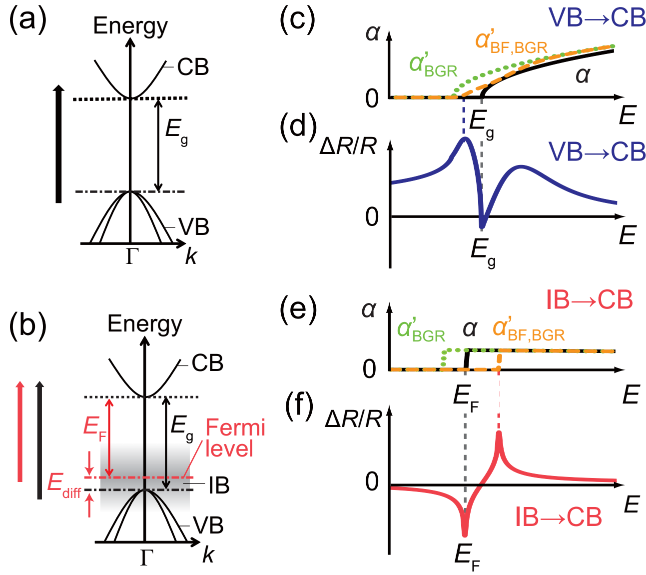

FIG. 1. (a), (b) Schematic illustration of the band structures of (a) GaAs and (b) GaMnAs with the optical transitions from the VB to the CB (black arrows) and from the IB to the CB (red arrow). The black dashed, red dashed-dotted, and black dashed-dotted horizontal lines represent the energy of the bottom of the CB, Fermi level, and the top of the VB, respectively. The gray region represents the IB region. (c), (e) Schematic absorption spectra; energy spectra of α (black solid curve), α'_{BGR} (green dotted curve), and $\alpha'_{\mathrm{BF,BGR}}$ (orange dashed curve) associated with the optical transitions (c) from the VB to the CB and (e) from the IB to the CB. (d), (f) Calculated $\Delta R/R$ spectrum associated with the optical transitions (d) from the VB to the CB and (f) from the IB to the CB.

allowing accurate analysis and estimations (see Sec. D of the SM [28]). The photoinduced change in the reflectivity (ΔR) divided by static reflectivity R,($\Delta R/R$), was detected with an accuracy of $\sim 10^{-4}$, using a lock-in technique as a function of the delay time t between the pump and probe pulses. Both the pump and probe pulses were linearly polarized.

For the pump-probe measurements, we used four $Ga_{1-x}Mn_xAs$ films ($x = 0.1\%$, 1%, 3%, and 6%) with thicknesses of 20 nm. The GaMnAs layer was grown on a 100-nm-thick GaAs buffer layer on a semi-insulating (SI) GaAs (001) substrate by low-temperature molecular-beam epitaxy. The $Ga_{0.999}Mn_{0.001}As$ film was paramagnetic; all other GaMnAs samples were ferromagnetic. The Curie temperatures of the ferromagnetic $Ga_{0.99}Mn_{0.01}As$, $Ga_{0.97}Mn_{0.03}As$, and $Ga_{0.94}Mn_{0.06}As$ films were 13, 38, and 110 K, respectively.

In this study, we investigated the electronic structure near the Fermi level of GaMnAs in the following scenario. In GaMnAs, there are absorption edges E_g and E_F, as shown in Fig. 1(b). Reflecting the photon energy (E) dependence of the density of states of the VB and IB, the intrinsic absorption (α) spectrum associated with the transition from the VB to the CB is parabolic [black curve in Fig. 1(c)], while that associated with the transition from the IB to the CB is step-like near $E = E_F$ [black curve in Fig. 1(e)] (more details can be found in Sec. B in the SM [28]). The photogenerated holes excited by pump-pulse illumination gradually relax to the top of the VB or to the Fermi level by emitting optical and acoustic

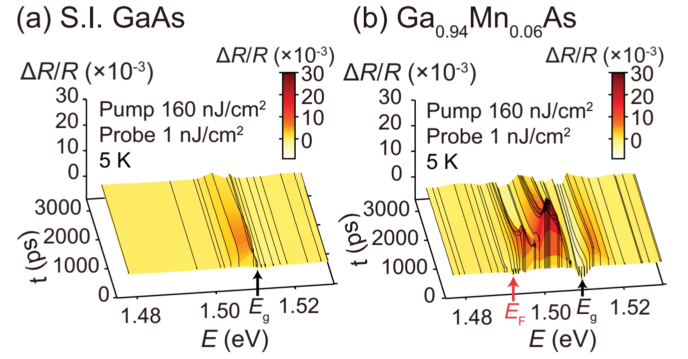

FIG. 2. (a), (b) Time evolution of $\Delta R/R$ (solid curves) as a function of the photon energy E measured at 5 K (a) for SI GaAs and (b) for $Ga_{0.94}Mn_{0.06}As$. The estimated E_g and E_F positions are indicated by the black and red arrows.

phonons on a time scale within $\sim$100 ps [24]. Then, the photogenerated carriers induce two effects on the intrinsic absorption spectrum α-E; one is the reduction of E_g via BGR [see $\alpha'_{\mathrm{BGR}} - E$ in Figs. 1(c) and 1(e)], and the other is the suppression of absorption due to state filling, i.e., BF. These two effects change the absorption [see $\alpha'_{\mathrm{BF,BGR}} - E$ in Figs. 1(c) and 1(e)] [25,27] and ΔR (see Sec. B of the SM [28]). Here, we define $\Delta\alpha$ as $\alpha - \alpha'_{\mathrm{BF,BGR}}$. The $\Delta R/R$ spectrum can be derived from the $\Delta\alpha$ spectrum using the Kramers-Kronig relationship given by

$$\frac{\Delta R}{R} \propto \frac{c\hbar}{\pi} \mathrm{P} \int_0^{\infty} \frac{\Delta\alpha}{E'^2 - E^2} dE', \qquad (1)$$

where c is the speed of light in vacuum, and P denotes the Cauchy principal value of the integral. The calculated $\Delta R/R$ spectra from Figs. 1(c) and 1(e) are shown in Figs. 1(d) and 1(f), respectively. We see that the $\Delta R/R$ spectra have a dip at the intrinsic absorption edge (E_g or E_F). By comparing the model calculation with the experimental results, we determined E_g and E_F for all samples used in this study, as described later. Note that we can neglect the diffusion effect of holes in our measurement time scale ($\sim$150 ps) due to the low mobility of holes in GaMnAs (see Sec. E of the SM [28]).

To confirm that the $\Delta R/R$ signals are enhanced near the absorption edges due to transient photocarriers, we first measured the time evolution of the light-induced reflectivity for the SI GaAs substrate [Fig. 2(a)] and the $Ga_{0.94}Mn_{0.06}As$ sample [Fig. 2(b)] as a function of E at 5 K. We see that $\Delta R/R$ signals appear near the absorption edges E_g (black arrows) and E_F (red arrow) just after pump-pulse illumination, and that the $\Delta R/R$ signals disappear over a nanosecond time scale. These features can be attributed to the generation and recombination dynamics of photocarriers trapped at As_{Ga} antisites and holes at the VB edge and/or Fermi level [29].

To determine E_F and E_g from the experimental $\Delta R/R$ spectra measured at 5 K and at $t = 166$ ps [plotted data in Fig. 3(c)], we analyzed these $\Delta R/R$ spectra with Eq. (1) [solid curves in Fig. 3(c)]. As a result of the fitting, we derived the absorption spectra shown in Fig. 3(a) and $\Delta\alpha = \alpha'_{\mathrm{BF,BGR}} - \alpha$ shown in Fig. 3(b) for $x = 6\%$. We clearly see absorption at E ranging from E_F to E_g [see the black solid curve in Fig. 3(a) and Sec. C in the SM [28] for other samples]. This is evidence

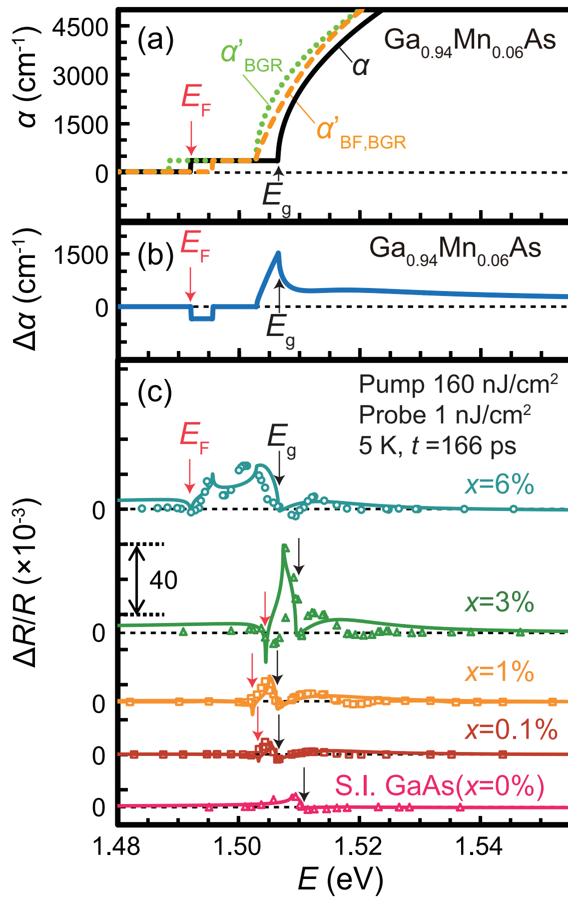

FIG. 3. (a) Absorption (α) spectra derived from the analysis of the TRS for $Ga_{0.94}Mn_{0.06}As$ (black curve). This is composed of the optical transitions from the IB to the CB ($E > E_F$) and from the VB to the CB ($E > E_g$). The absorption spectrum when assuming that only the BGR occurs is shown by the (green) dotted curve. It is changed to the one shown by the (orange) dashed curve due to the BF in addition to the BGR. (b) $\Delta\alpha$ spectrum obtained for the $Ga_{0.94}Mn_{0.06}As$ film. (c) $\Delta R/R$ spectra measured at 5 K for the SI GaAs substrate and for the $Ga_{1-x}Mn_xAs$ films ($x = 0.1\%$, 1%, 3%, and 6%) at $t = 166$ ps (plotted data). The solid curves are the fitting curves.

of the presence of the IB inside the band gap in GaMnAs. In Fig. 3(c), E_F (red arrows) has a lower energy than E_g (black arrows) for all x. This indicates that the Fermi level exists in the band gap for all x.

Figure 4 shows the x dependence of the energy difference E_{diff} between the Fermi level and the top of the VB [see Fig. 1(b)] obtained from the data shown in Fig. 3(c). We found that E_{diff} increases with increasing x, as shown by the red diamonds in Fig. 4. These results are consistent with the data obtained by the resonant tunneling study in the region of $x > 1\%$ (blue circles in Fig. 4) [4] that revealed anomalous

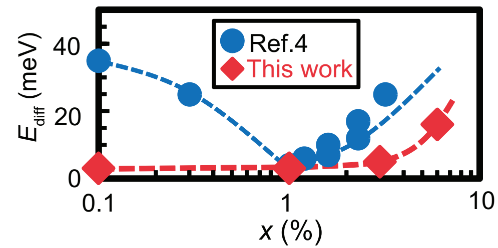

FIG. 4. x dependence of E_{diff} (red diamonds). The blue solid circles are the values reported in Ref. [4].

behavior of the Fermi level around $x = 1\%$; E_{diff} decreases in the region of $x < 1\%$, while E_{diff} increases in the region of $x > 1\%$ [4]. The reason for the difference in E_{diff} when $x < 1\%$ between this work and Ref. [4] may be explained by the following scenario. When $x < 1\%$, GaMnAs is insulating, and holes are localized near the Mn atoms. Thus, the optical transition probability from the localized impurity states to the CB is small, due to the small wave-function overlap between the localized photoholes and the photoelectrons. This leads to the small signal for $x = 0.1\%$ [Fig. 3(c)] and may make the correct derivation of the fitting parameters difficult. In the region of $x > 1\%$, the values of E_{diff} obtained in our study are slightly smaller than those obtained in previous reports [3,4]. This difference may be caused by the screening effect of the potential of the Mn atoms on photoexcited carriers or the small overestimation of E_{diff} in the resonant tunneling study due to series resistance. The most important feature of our results is that our TRS measurements successfully reproduced the anomalous behavior of the Fermi level when $x > 1\%$.

In summary, we studied the electronic structure near the Fermi level in GaMnAs by measuring the TRS using a low pump power (160 nJ/cm^2) at a high energy resolution (~0.5 meV). The data show light-induced changes in the reflectivity spectra, attributed to BGR and BF. We reproduced the observed $\Delta R/R$ spectra in a calculation based on our band structure model, and found that the Fermi level is located in the band gap. We found Mn-induced electronic states near the Fermi level inside the band gap in all GaMnAs films studied here. This confirms that spin-polarized IB holes stabilize the ferromagnetism in GaMnAs.

This work was partially supported by Grants-in-Aid for Scientific Research including Specially Promoted Research, Project for Developing Innovation Systems of Ministry of Education, Culture, Sports, Science and Technology, Japan, and Spintronics Research Network of Japan. T.I. was supported by the Japan Society for the Promotion of Science through the Program for Leading Graduate Schools (MERIT). T.I. thanks the Japan Society for the Promotion of Science Research Fellowship Program for Young Scientists for support.

[1] T. Dietl, H. Ohno, F. Matsukura, J. Cibert, and D. Ferrand, Science **287**, 1019 (2000).

[2] M. Tanaka, S. Ohya, and P. N. Hai, Appl. Phys. Rev. **1**, 011102 (2014).

[3] S. Ohya, K. Takata, and M. Tanaka, Nat. Phys. **7**, 342 (2011).

[4] I. Muneta, H. Terada, S. Ohya, and M. Tanaka, Appl. Phys. Lett. **103**, 032411 (2013).

[5] K. Ando, H. Saito, K. C. Agarwal, M. C. Debnath, and V. Zayets, Phys. Rev. Lett. **100**, 067204 (2008).
[6] H. Terada, S. Ohya, and M. Tanaka, Appl. Phys. Lett. **106**, 222406 (2015).
[7] M. Kobayashi, I. Muneta, Y. Takeda, Y. Harada, A. Fujimori, J. Krempaský, T. Schmitt, S. Ohya, M. Tanaka, M. Oshima, and V. N. Strocov, Phys. Rev. B **89**, 205204 (2014).
[8] T. Matsuda and H. Munekata, Phys. Rev. B **93**, 075202 (2016).
[9] S. Kim, E. Oh, J. U. Lee, D. M. Kim, S. Lee, and J. K. Furdyna, Appl. Phys. Lett. **88**, 262101 (2006).
[10] M. Dobrowolska, K. Tivakornsasithorn, X. Liu, J. K. Furdyna, M. Berciu, K. M. Yu, and W. Walukiewicz, Nat. Mater. **11**, 444 (2012).
[11] M. Yildirim, S. March, R. Mathew, A. Gamouras, X. Liu, M. Dobrowolska, J. K. Furdyna, and K. C. Hall, Phys. Rev. B **84**, 121202(R) (2011).
[12] A. Patz, T. Li, X. Liu, J. K. Furdyna, I. E. Perakis, and J. Wang, Phys. Rev. B **91**, 155108 (2015).
[13] T. Jungwirth, P. Horodyská, N. Tesařová, P. Němec, J. Šubrt, P. Malý, P. Kužel, C. Kadlec, J. Mašek, I. Němec, M. Orlita, V. Novák, K. Olejník, Z. Šobáň, P. Vašek, P. Svoboda, and J. Sinova, Phys. Rev. Lett. **105**, 227201 (2010).
[14] T. Jungwirth, J. Sinova, A. H. MacDonald, B. L. Gallagher, V. Novák, K. W. Edmonds, A. W. Rushforth, R. P. Campion, C. T. Foxon, L. Eaves, E. Olejník, J. Mašek, S.-R. E. Yang, J. Wunderlich, C. Gould, L. W. Molenkamp, T. Dietl, and H. Ohno, Phys. Rev. B **76**, 125206 (2007).
[15] O. Yastrubchak, J. Żuk, H. Krzyżanowska, J. Z. Domagala, T. Andrearczyk, J. Sadowski, and T. Wosinski, Phys. Rev. B **83**, 245201 (2011).
[16] T. de Boer, A. Gamouras, S. March, V. Novák, and K. C. Hall, Phys. Rev. B **85**, 033202 (2012).
[17] C.-H. Liu, N. M. Dissanayake, S. Lee, K. Lee, and Z. Zhong, ACS Nano **6**, 7172 (2012).
[18] R. S. Joshya, A. J. Ptak, R. France, A. Mascarenhas, and R. N. Kini, Phys. Rev. B **90**, 165203 (2014).
[19] R. Bouzerar and G. Bouzerar, Europhys. Lett. **92**, 47006 (2010).
[20] A. X. Gray, J. Minár, S. Ueda, P. R. Stone, Y. Yamashita, J. Fujii, J. Braun, L. Plucinski, C. M. Schneider, G. Panaccione, H. Ebert, O. D. Dubon, K. Kobayashi, and C. S. Fadley, Nat. Mater. **11**, 957 (2012).
[21] J. Okabayashi, A. Kimura, O. Rader, T. Mizokawa, A. Fujimori, T. Hayashi, and M. Tanaka, Phys. Rev. B **64**, 125304 (2001).
[22] S. Ohya, I. Muneta, P. N. Hai, and M. Tanaka, Phys. Rev. Lett. **104**, 167204 (2010).
[23] I. Muneta, S. Ohya, H. Terada, and M. Tanaka, Nat. Commun. (to be published).
[24] J. Shah, *Ultrafast Spectroscopy of Semiconductors and Semiconductor Nanostructures*, Springer Series in Solid-State Sciences Vol. 115 (Springer, Berlin, 1999).
[25] S. S. Prabhu and A. S. Vengurlekar, J. Appl. Phys. **95**, 7803 (2004).
[26] C. V. Shank, R. L. Fork, R. F. Leheny, and J. Shah, Phys. Rev. Lett. **42**, 112 (1979).
[27] B. R. Bennett, R. A. Soref, and J. A. D. Alamo, IEEE J. Quantum Electron. **26**, 113 (1990).
[28] See Supplemental Material at http://link.aps.org/supplemental/10.1103/PhysRevB.93.241303 for energy resolution (Sec. A), derivation of the fitting curves and fitting parameters (Sec. B), fitting results (Sec. C), pump-power dependence (Sec. D), and diffusion effect of holes (Sec. E).
[29] M. Haiml, U. Siegner, F. Morier-Genoud, U. Keller, M. Luysberg, P. Specht, and E. R. Weber, Appl. Phys. Lett. **74**, 1269 (1999).